NANO LETTERS

LETTER

pubs.acs.org/NanoLett

Localized Joule Heating As a Mask-Free Technique for the Local Synthesis of ZnO Nanowires on Silicon Nanodevices

C. C. Chen,[†,‡] Y. S. Lin,[†] C. H. Sang,[†] and J.-T. Sheu*[,†]

[†]Institute of Nanotechnology/Materials Science and Engineering, National Chiao Tung University, 1001 Ta-Hsueh Road, Hsinchu 30050, Taiwan

[‡]National Chip Implementation Center, National Applied Research Lab, 7F, No. 26, Prosperity Road 1, Science Park, Hsinchu 300, Taiwan

Supporting Information

ABSTRACT: We report a mask-free technique for the local synthesis of ZnO nanowires (NWs) on polysilicon nanobelts and polysilicon NW devices. First, we used localized joule heating to generate a poly(methyl methacrylate) (PMMA) nanotemplate, allowing the rapid and self-aligned ablation of PMMA within a short period of time (ca. 5 μs). Next, we used ion-beam sputtering to prepare an ultrathin Au film and a ZnO seed layer; a subsequent lift-off process left the seed layers selectively within the PMMA nanotemplate. Gold nanoparticles and ZnO NWs were formed selectively in the localized joule heating region.

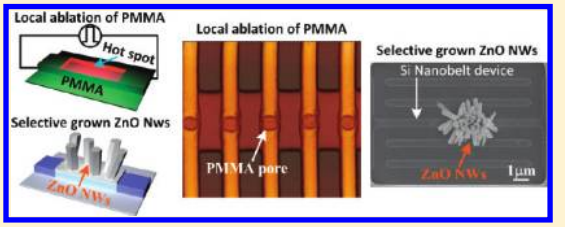

KEYWORDS: Nanobelt, nanowire, nanoparticle, ZnO, joule heating

Much effort has been exerted in the preparation of one-dimensional materials, nanowires (NWs), and nanotubes (NTs) due to their characteristics being inherently different from those of their corresponding bulk materials.[1] Single-crystalline semiconductor NWs grown vertically on a substrate have a variety of potential applications, for example, in self-powered devices,[2,3] field-emission devices,[4] sensors,[5,6] and light-emitting diodes.[7] The perfect positioning of NWs (or carbon NTs) perpendicular to one another can improve the performance of devices and increase the flexibility of their design and integration.[8−10] The manipulation of these NWs or carbon NTs into desired positions has been accomplished typically through the assistance of microfluidic flow or the tip of a scanning probe microscopy (SPM) system.[11,12] Although the manipulation of single NWs by SPM tips is widespread, it is painstaking and time-consuming technique task for the simultaneous manipulation of many NWs. Moreover, this approach does not enable the mutual registration of elliptical out-of-plane NWs. A general strategy for positioning the growth of vertically aligned NWs is through positioning deposition with the assistance of a catalyst or seed layer. Several photolithography,[13] laser interference lithography,[14] nanosphere lithography,[15] and nanoimprint lithography[16] techniques have been developed for the selective deposition of metal arrays as catalysts for large-area patterning of NWs. Nevertheless, the ability to grow NWs precisely on other NWs will still require the development of a new scalable technique. Dip-pen nanolithography (DPN), which provides extremely precise alignment, has been used to generate nanostructures from several metal materials (Au, Ag, Pd).[17] The use of DPN for the direct patterning of gold nanoparticles (AuNPs) was recently demonstrated.[18] The major drawback of DPN is that it is a time-consuming procedure. Although electron beam lithography (EBL) can be used to define patterns of exposed seeds or catalyst layers for subsequent growth of NWs,[19] this technique is also time-consuming and expensive.

To achieve controllable growth of highly ordered and self-aligned NWs at desired positions on other NWs, it will be necessary to develop feasible methods for the self-alignment of patterned catalysts on NWs without the need for lithography processes. Suspended polysilicon bridge was reported and used as a microheater for synthesis of nanowires.[20−22] In order to lower the operation voltage for creating higher temperature, the whole polysilicon microstructures were usually heavily doped. However, the totally heavily doped microstructure does not generate heat in a specific region. To confine heat generation at a local region, microstructure with a lightly doped region was presented. To our best knowledge, local synthesis of nanowires (footprint of grown region <1 μm^2) using a polysilicon microheater with a lightly doped region has never been reported. The challenges are two-fold; precise control of low-level doping concentration in polysilicon nanobelt is difficult. Also, the dimension of lightly doped region is very hard to scale down to submicrometer due to the dopant out-diffusion from the highly doped two ends during dopant activation process. In this letter, we describe a facile approach, using localized joule heating, for precisely self-aligning catalysts on polysilicon nanobelts (NBs) and NWs, allowing the subsequent growth of ZnO NWs on the catalyst sites on the polysilicon NBs and NWs.

Received: July 25, 2011
Revised: October 11, 2011
Published: October 18, 2011

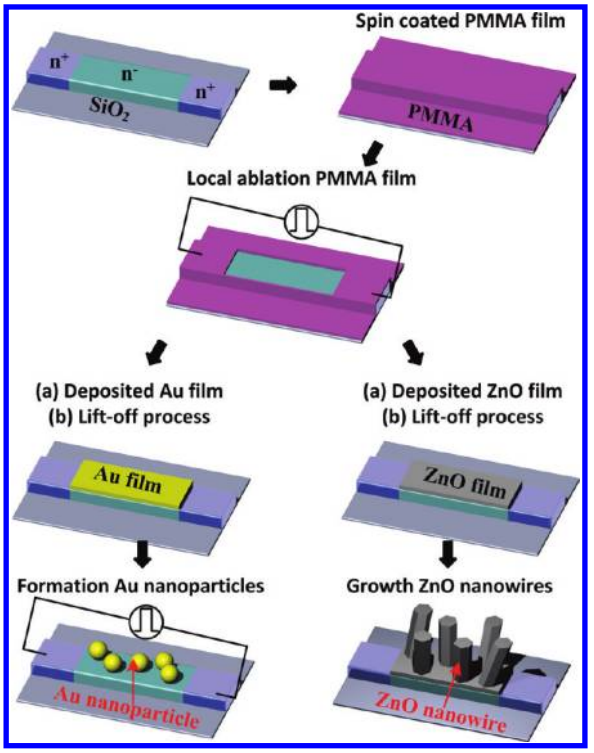

Figure 1. Schematic representation of the fabrication of self-aligned and precisely formed AuNPs and grown ZnO NWs upon the lightly doped region of a polysilicon nanobelt device.

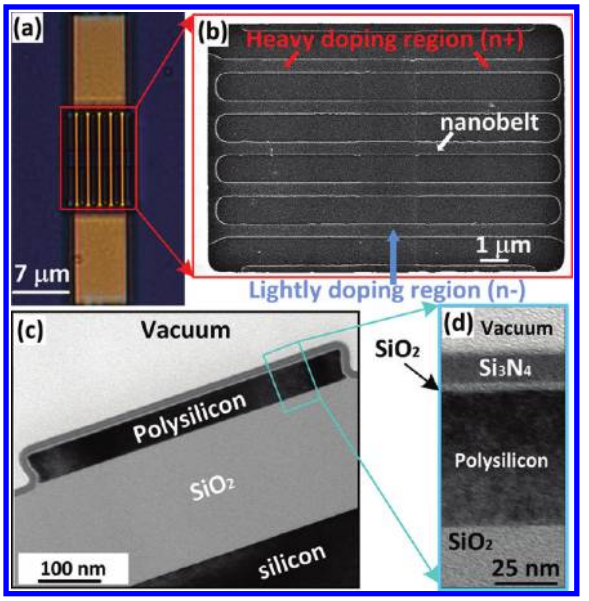

Figure 2. (a,b) Top-view (a) optical and (b) SEM images of a typical polysilicon nanobelt device; the polysilicon nanobelts were ca. 12.6 μm long. (c,d) Cross-sectional TEM images of a single polysilicon nanobelt taken after FIB milling; the thicknesses of the silicon nitride, silicon dioxide, and polysilicon layers were ca. 12, 3, and 50 nm, respectively.

Figure 1 provides a schematic representation of the process we developed to precisely grow ZnO NWs and form AuNPs at defined positions on a polysilicon nanodevice. First, we coated a poly(methyl methacrylate) (PMMA) thin film onto a sample featuring polysilicon nanodevices. Next, the application of a single pulse voltage in the polysilicon nanodevice selectively and rapidly removed the PMMA polymer from the lightly doped region of the polysilicon nanodevice. In the third step, gold and ZnO ultrathin films were deposited through ion-beam sputtering; a subsequent lift-off process completely and selectively removed the PMMA thin film while leaving the ultrathin gold and ZnO seeds intact. In case 1, we performed localized joule heating by applying a single voltage pulse for a very short period of time, thereby annealing the ultrathin gold film (2 nm); the heating energy was sufficiently high to totally melt the gold film and form AuNPs randomly. In case 2, we used a hydrothermal method to grow ZnO NWs from the ZnO seed layer.

We fabricated polysilicon nanodevices on a Si wafer featuring a thermal oxide layer; the Supporting Information provides a detailed process flow map for the fabrication of the polysilicon nanobelt device. Figure 2a presents an optical image of a typical polysilicon nanobelt device, which comprised multiple polysilicon nanobelts. The doping profile along the polysilicon nanobelt is a key factor affecting the generation of localized hot spots. To confirm the size of the hot spot, we performed a two-step implantation process. The polysilicon nanobelts were uniformly and lightly doped through a first ion implantation process; a second ion implantation process was then performed to yield good ohmic contacts and to define the length of the lightly doped region of the polysilicon nanobelt. Figure 2b presents a top-view scanning electron microscopy (SEM) image of a polysilicon nanobelt device. The length of the polysilicon nanobelt device was set at 12.6 μm; a gap of 1 μm separated each device. For transmission electron microscopy (TEM) analysis, a focused ion beam (FIB) was applied in the direction perpendicular to the polysilicon nanobelt. Figure 2c provides close-up TEM cross-sectional views of a polysilicon nanobelt having a channel width of 420 nm. Figure 2d displays a high-resolution TEM image of a polysilicon nanobelt capped with a bistacked layer (thicknesses of SiO_2 and Si_3N_4 layers: ca. 3 and 12 nm, respectively).

We used a noncontact thermal infrared (IR) microscope (Infrascope II, Quantum Focus Instruments) to investigate the surface temperature distribution of a polysilicon nanobelt device under various applied voltages. Figure 3a presents a series of thermal IR images of a polysilicon nanobelt device operated under various voltages. Initially, the temperature on the thermally isolated SiO_2 layer and the unexcited polysilicon nanobelt device were close to the stage temperature of 70 °C. When the polysilicon nanobelt device was stressed at 42 V, we observed a surface temperature of greater than 300 °C. Figure 3b presents a series of thermal radiation images of a polysilicon nanobelt device under various operating voltages. The illuminating light from the optical microscope was turned off during the observation; the exposure time was 4 s. The bright spots glowed only in the lightly doped regions of the polysilicon nanobelt device; the size was enlarged and the brightness enhanced upon increasing the bias. The orange glow could be switched instantaneously by controlling the voltage supply, indicating a very short response time. Moreover, the color of the orange glow was indicative of a local temperature of over 1000 °C during the joule heating process.[22,23] Figure 3c presents an optical image of polysilicon nanobelt devices before applying a voltage; Figure 3d reveals the broken polysilicon nanobelt devices after stressing at a bias greater than 42 V. These images suggest that the local temperature of the polysilicon nanobelt device reached the melting point of polysilicon (>1400 °C)[21] under a bias of 42 V. Device failure can also be attributed to thermally induced stress during heating.[24]

dx.doi.org/10.1021/nl202539m |*Nano Lett.* 2011, 11, 4736–4741

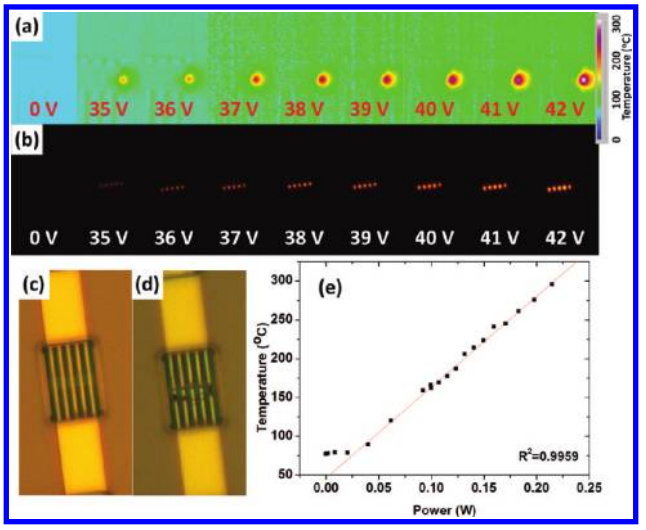

Figure 3. (a) IR images of a polysilicon nanobelt device at various applied voltages. (b) Thermal radiation images of polysilicon nanobelt devices, captured using a charge-coupled device (CCD) under various applied voltages with the illuminating light of the microscope turned off. (c,d) Optical images of this particular device (c) before and (d) after failure. (e) Maximum surface temperature plotted with respect to the dissipation joule heating power, estimated using an IR microscope.

Notably, the surface temperature measured using a noncontact thermal IR microscope was significantly lower than the real surface temperature, presumably because the size of the hot spot (ca. 0.5 μm) was smaller than the spatial resolution of the IR thermal image (ca. 2.8 μm) when using a 15× objective; accordingly, the temperature was averaged out, so that the temperature appeared lower when observed using the infrascope. Figure 3e displays the maximum surface temperature of the polysilicon nanobelt devices as function of the joule heating power. If the heat released is due to current flowing through a polysilicon nanobelt, then the heat measured should follow Joule's law

$$P = I^2R = IV$$

where P is the joule heating power, I is the current flowing through the polysilicon nanobelt device, R is its resistance, and V is the voltage applied to the contact pad. The maximum surface temperature of our polysilicon nanobelt device exhibited a linear dependence on the dissipated joule heating power.

We also simulated the surface temperature distribution of the polysilicon nanobelt devices using three-dimensional (3D) finite-element analysis (COMSOL Multiphysics 4.2). Prior to simulation, we had to determine the temperature coefficient of resistance (TCR) of the polysilicon nanobelt. To do so, we placed a polysilicon nanobelt device on the thermal chuck for calibration and varied the temperature of the thermal chuck from 25 to 300 °C (see Figure S2 in Supporting Information).

The glass transition temperature of PMMA ranges from 95 to 106 °C with a melting point of approximately 160 °C.[25] Figure 4a shows the atomic force microscopy (AFM) images of the PMMA morphology after applying a single electric pulse (duration, 5 μs; amplitude, 32−46 V, step = 2 V) to the polysilicon nanobelts. When the applied voltage is small than 30 V, the surface morphology of the polymer remained unchanged (results not shown). It reveals that the surface temperature of lightly doped region was less than the melting temperature of PMMA. Upon increasing

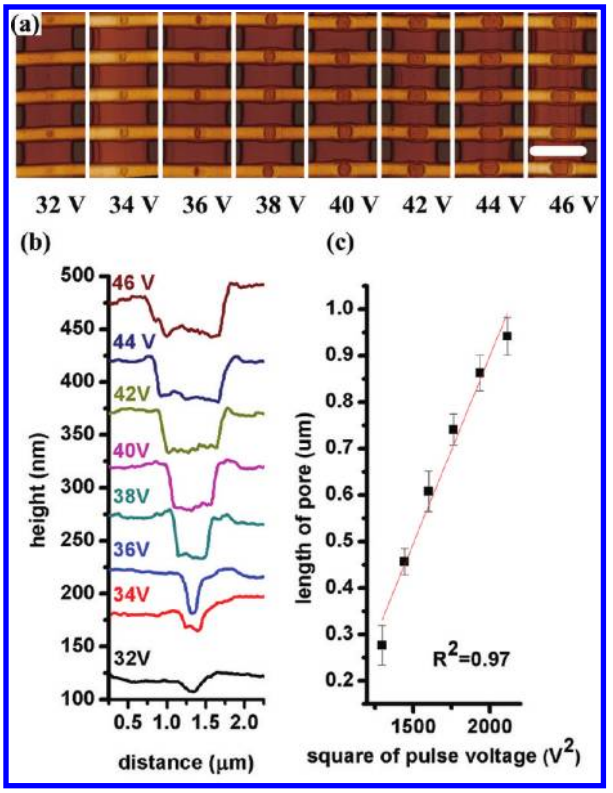

Figure 4. (a) AFM images of the PMMA morphology after applying single electrical pulse (duration, 5 μs; amplitude, 32 to 46 V, step = 2 V). (b) PMMA cross-sectional profiles of the middle polysilicon nanobelt along the long axis. (c) Plot of pore size along the long axis versus applied power. Scale bar = 2 μm.

the amplitude of pulse voltage from 32 to 34 V, the local temperature rose rapidly, a cavity pit appeared upon the lightly doped region. It is worth to note that the cavity pit depth was smaller than the thickness of spun PMMA film. The PMMA film was partially ablated, as shown in Figure 4b. Upon continuously increasing the amplitude of the pulse voltage to higher than 34 V, the PMMA film above the lightly doped region was ablated entirely, leaving the channel surface exposed. When the surface temperature of lightly doped region is smaller than the boiling point of PMMA, the pores formation process is mainly dominated by melting mechanism. On the other hand, the oxidation mechanism dominates in pore formation process as the surface temperature larger than the boiling temperature of PMMA.[26] The pore formed an elliptical shape; the growth rate of the pore was faster along the channel of the nanobelt than it was along its short axis. Because the thermal conductivity of SiO_2 is lower than the thermal conductivity of polysilicon, the heat did not dissipate readily from the nanobelts to the surrounding regions, due to thermal insulation between the nanobelts. This phenomenon is consistent with the simulation data. Typically, the PMMA was totally ablated above 400 °C in a thermogravimetric analysis (TGA) experiment. We assume that PMMA thin film was totally ablated when the surface temperature of nanobelt heater higher than 400 °C. The pore shape (as shown in Figure 4a) closely resembles with the thermal distribution region for temperature larger than 400 °C in COMSOL simulation. (see Figure S3, Supporting Information). Nevertheless, the length of thermal distribution region (temperature larger than 400 °C) from simulation

dx.doi.org/10.1021/nl202539m |Nano Lett. 2011, 11, 4736–4741

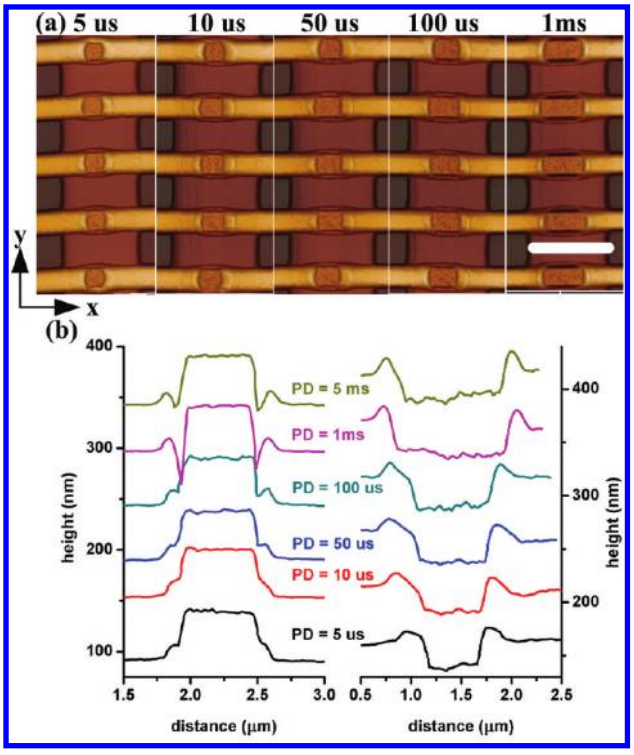

Figure 5. (a) AFM images of the PMMA pores after applying a peak voltage of 40 V at different pulse widths (pulse duration (PD): 5 μs to 1 ms). (b) PMMA cross-sectional profiles in the direction of *y*-axis (left figure) and *x*-axis (right figure) of the middle polysilicon nanobelt. Scale bar = 2 μm.

data (ca. 2 μm) is about 3.3-fold larger than the length of PMMA pore (ca. 0.6 μm). It is attributed that the real length of lightly doping region of polysilicon nanobelt is smaller than 2 μm due to the dopant out-diffusion from the highly doped regions. Figure 4c shows plot of pore length along the polysilicon nanobelt versus applied power, the relationship between the length of pore and the square of pulse voltage is almost linear indicating that power dissipation in lightly doped region follows the Joule's law and the volume of ablated PMMA is linearly related to the input power.

Because of the limitation of design rule in device fabrication, we only minimized the nanobelt to nanobelt spacing and length of lightly doped region in the nanobelt to 1 and 2 μm, respectively. Figure 5a presents AFM images of the PMMA pores after applying a peak voltage of 40 V at different pulse widths. PMMA pore sizes shrank down to ca. 380 nm in long-axis direction of polysilicon nanobelt at a pulse width of 5 μs. Figure 5b shows cross-sectional PMMA profiles in the direction of *y*-axis (short-axis) and *x*-axis (long-axis) of the middle polysilicon nanobelt. PMMA pore width in the short-axis elongated from 650 $\pm$ 32 to 739 $\pm$ 27 nm as the pulse duration increases from 5 μs to 1 ms. These results indicate that the pore to pore spacing between adjacent nanobelts were shrunk from 873 $\pm$ 37 to 809 $\pm$ 13 nm. Together with the temperature distribution profile resulted from COMSOL simulation, the margin of wire to wire spacing could be shrunk down to 200 nm under current operation conditions.

Next, we used ion-beam sputtering to deposit a 2 nm thick gold film; a subsequent lift-off process removed the PMMA thin film, leaving the ultrathin gold film locally (see Figure S4, Supporting Information). Again, we performed localized joule heating using a voltage pulse having an amplitude of 40 V for a duration of 50 μs. Figure 6a,b displays typical SEM images of the as-grown ultrathin gold film and that annealed through localized joule heating, respectively. The heating energy was sufficiently high to melt the gold film completely and form AuNPs randomly. The uniformity of the size and density of AuNPs was strongly dependent on the uniformity of the annealing temperature. Further optimization of the doping profile in the polysilicon could enhance the uniformity of the temperature distribution. Furthermore, diffusion is a great concern in high temperature processing because any C or Au atoms that diffuse into the active channel of the polysilicon nanobelt usually undermine the device's electrical characteristics. In this study, they observed no obvious diffusion of carbon atoms into the silicon NW within short periods of time (< 1 min).[27] Therefore, under the very short time (50 μs) that we employed for processing, the diffusion of C atoms can be ignored. The AuNPs that formed stabilized the atomic cluster in a spherical shape at a minimum energy state, rather than allowing diffusion through the stacked layer of the SiO_2/Si_3N_4 thin film, which functioned as an adequate diffusion barrier that also minimized the diffusion of Au atoms penetrating into the polysilicon nanobelt. The diffusion length, defined using the equation[29]

$$L_D = (Dt)^{1/2}$$

where D is the diffusion constant, increased upon increasing the diffusion time or temperature as a result of the increased diffusion length. The diffusion coefficient of Au atoms in silicon oxide at 1000 °C has been reported to be 5.5×10^{-15} cm^2 s^{-1}.[28] Therefore, using the formula above, we estimated the diffusion length of Au atoms within the pulse duration at 1000 °C to be approximately 5.2 Å. From the TEM image and EDX results (see Figure S5, Supporting Information), no obvious signals for Au atoms were evident within the stacking layer or the polysilicon nanobelts, confirming that the diffusion of Au atoms was negligible. Therefore, the short cycle time required for annealing through joule heating has the advantage of reducing the thermal budget and manufacturing cost.

Using the method described above, it is also possible to realize the selective growth of ZnO NWs at designated positions on the polysilicon nanobelt devices through selective patterning of the seed layers. AuNPs have been employed previously as catalysts to initiate the growth of ZnO NWs using metal organic vapor-phase epitaxy[29] and physical vapor deposition.[30] In this study, we chose a hydrothermal method[31] to synthesis the ZnO NWs; this method has the main advantage of providing ZnO NWs through a simple process performed at a low growth temperature. The synthesis of ZnO NWs using this hydrothermal method typically requires a thin ZnO film as the seed layer; therefore, we replaced the AuNPs by a ZnO seed layer. First, the ZnO seed layer was deposited selectively on the polysilicon nanobelt device; next, ZnO NWs were grown using the hydrothermal method with the ZnO seed layer as the growth catalyst. Figure 6c,d presents typical SEM images of ZnO NWs grown selectively on single and multiple polysilicon nanobelt devices, respectively. The ZnO NWs did not grow on the other regions because of the lack of nucleation sites. Most of the ZnO NWs were formed nearly vertically in the middle of the patterned region, except for some positioned on the edges of the ZnO seed layer pattern. The different sizes of the ZnO NWs possibly resulted from the patterned ZnO seed layer consisting of many randomly size ZnO NPs.

Figure 7a presents a cross-sectional TEM image of a polysilicon NW channel having a width of approximately 83 nm and a

dx.doi.org/10.1021/nl202539m |*Nano Lett.* 2011, 11, 4736–4741

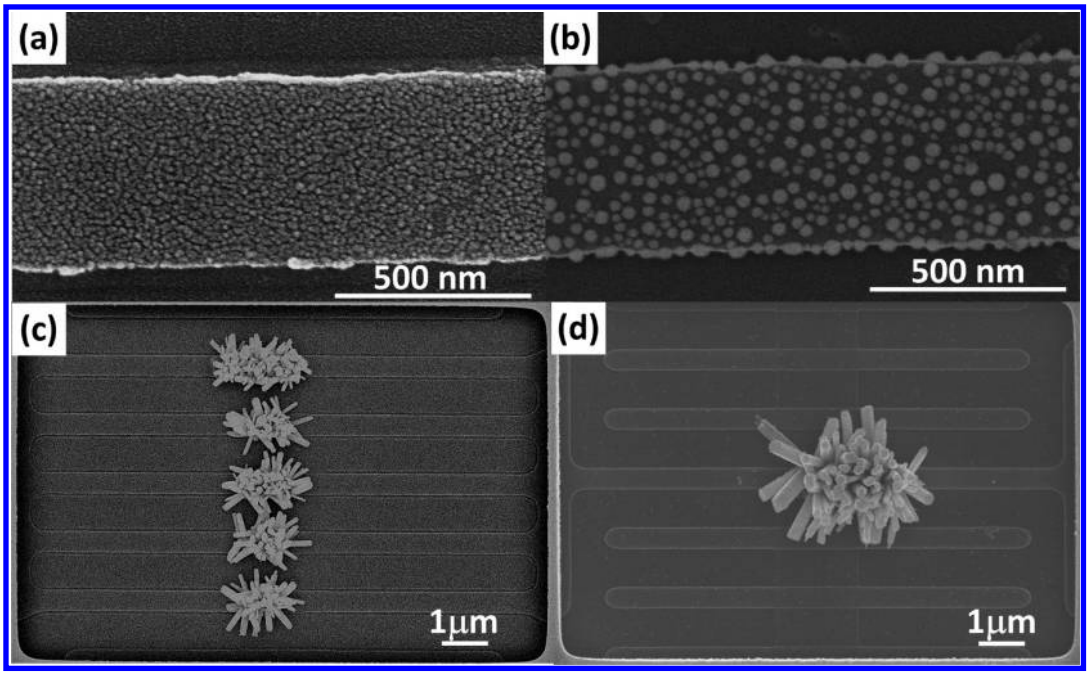

Figure 6. (a,b) Typical SEM images of ultrathin Au films: (a) as-grown; (b) annealed through localized joule heating. (c,d) Typical SEM images of ZnO NWs selectively grown on (c) multiple and (d) single polysilicon nanobelt devices.

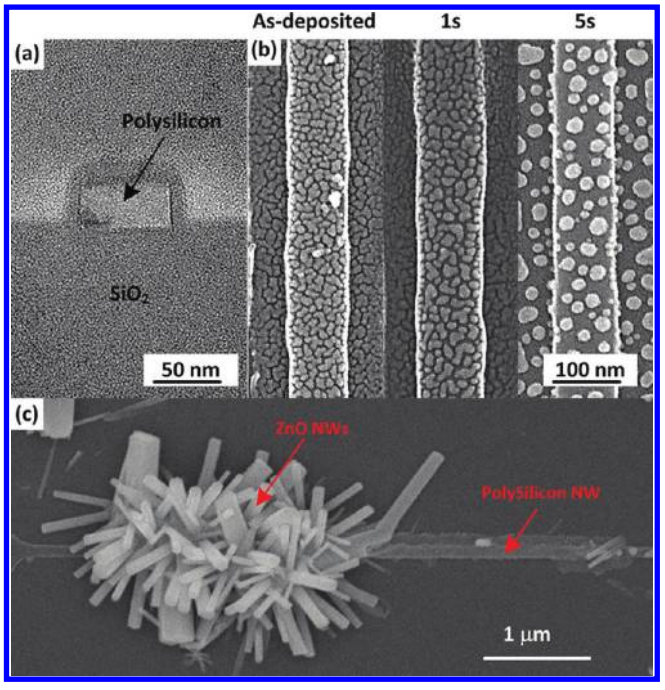

Figure 7. (a) Cross-sectional TEM image of a polysilicon NW. (b) Typical SEM images of ultrathin Au films annealed through local joule heating for various periods of time. (c) Typical SEM image of ZnO NWs grown selectively on a polysilicon NW device.

height of approximately 43 nm. The average resistance and TCR of a single polysilicon NW and were 2.03 ± 0.62 MΩ and -1669 ± 196 ppm/°C, respectively. Figure 7b presents SEM images of a 2 nm thick Au film on a polysilicon NW annealed through joule heating for various periods of time (from 0 to 5 s). The dimensions of the AuNPs increased upon increasing the annealing time. A longer annealing time allowed mass transport of small clusters across the surface to form larger clusters. Despite the resistance of a polysilicon NW being approximately 10 times higher than that of a nanobelt device, the time required for both localized joule heating and annealing of the Au film were much longer than expected; the reason for this behavior remains unclear and requires further study. Moreover, Wei et al. suggested that, because competition exists between ZnO growth and nucleus formation, when the dimensions of the seed layer pattern were smaller than the critical size, individual ZnO particles would grow on the seed layer pattern.[14] In this present study, the typical width of the pattern of the ZnO seed layer was approximately 100−200 nm, considerably smaller than that reported by Wei's group. Unfortunately, the multiple ZnO NWs that grew on the devices did not merge together to form a thicker ZnO NW, as revealed in Figure 7c. These results are different from those from a previous results;[19] further study will be required to provide an explanation.

We also investigated the growth of ZnO nanowires out of the surface of nanobelt device is beneficial to immobilization efficiency of target molecules in solution. Nanobelt devices with NTA-modified ZnO nanowires and nanobelts with NTA-modified ZnO thin film were investigated by using FITC-labeled BSA as the target. Supporting Information Figure S6 reveals that polysilicon nanobelt device with ZnO nanowires exhibited a dramatically improvement in fluorescent intensity relative to that of its counterpart device. This enhancement is also unambiguously contributed from the high specific surface area (ZnO nanowires act as antenna). A related research was reported recently by Jiang et al. on synthesis of 3D branched nanowire heterostructures.[32] They also demonstrated that Au branches can act as "antenna" in a Si/Au-branch NW sensor and exhibited an excellent sensitivity and selectivity compared to that of bare SiNW device. Because sensitivity of polysilicon nanobelt was not optimized in this study, we did not investigate characteristics of electrical measurement in sensing applications. However, the

dx.doi.org/10.1021/nl202539m |*Nano Lett.* 2011, 11, 4736–4741

sensitivity of NW-FET has been significantly enhanced when operating in the subthreshold region.[33] When NW-FET operated in this region, the Debye length of silicon, λ_{Si}, is larger than the radius of nanowire, which resulted in a dramatically enhancement in sensitivity due to whole active channel of NW is gated by the change of surface potential. This also implies that the sensitivity of NW-FET can be significantly improved by lowering the channel doping level so that the Debye length of silicon is larger than the channel thickness. We also estimated that the lightly doped region of nanobelt (polysilicon thickness = 59.5 nm) would be fully gated by surface charges when the doping level is reduced to ca. 5×10^{15}cm^{-3} ($\lambda_{Si} \approx 60$ nm). The resistance of nanobelt device is ca. 375 kΩ at this doping level. On the other hand, the total energy for PMMA ablation in time t can be estimated by $Q = t(V^2/R)$ and was ~0.615 μJ in forming a pore with pore length ca. 0.6 μm along the polysilicon nanobelt as shown in Figure 4. The surface temperature at lightly doped region (doping level of 5×10^{15} cm^{-3}) was higher than 400 °C in 5 μs under a pulse bias of 65 V (see Figure S7, Supporting Information). And, localized Joule heating could provide energy of 0.615 μJ in ~54.8 μs so that selective PMMA ablation is expected to fulfill.

In summary, we have performed the local synthesis of ZnO NWs on polysilicon nanobelts and polysilicon NW devices. We developed a facile approach for generating a PMMA template on the lightly doped regions of these devices through localized joule heating for a short period of time (<5 μs). After PMMA ablation, we used ion-beam sputtering to prepare ultrathin Au films and ZnO films; subsequent lift-off processing selectively left behind the gold and ZnO films. Annealing for just 50 μs was required to transform the ultrathin Au film into AuNPs in nanobelt devices; therefore, relative to conventional rapid thermal annealing techniques (e.g., rapid thermal annealing, laser annealing), our proposed method is approximately 4 orders of magnitude faster. Finally, by controlling the location of ZnO seeds, we could also precisely control the growth of ZnO NWs. We suspect that this simple and economical approach would be applicable in many fields, especially nanobiosensing, in which the sensing response and sensitivity of the biosensor can be improved through antenna effect.

■ ASSOCIATED CONTENT

Ⓢ Supporting Information. Additional information and figures. This material is available free of charge via the Internet at http://pubs.acs.org.

■ ACKNOWLEDGMENT

We thank the National Science Council and the MOE-ATU Program in Taiwan for financial support. We also thank Professor Da-Jeng Yao of Institute of NanoEngineering and MicroSystems, National Tsing Hua University, Taiwan for the assistance in infrared microscopic work.

■ REFERENCES

(1) Xia, Y. N.; Yang, P. D.; Sun, Y. G.; Wu, Y. Y.; Mayers, B.; Gates, B.; Yin, Y. D.; Kim, F.; Yan, Y. Q. *Adv. Mater.* **2003**, *15*, 353.
(2) Law, M.; Greene, L. E.; Johnson, J. C.; Saykally, R.; Yang, P. D. *Nat. Mater.* **2005**, *4*, 455.
(3) Wang, Z. L.; Song, J. H. *Science* **2006**, *312*, 242.
(4) Lee, C. J.; Lee, T. J.; Lyu, S. C.; Zhang, Y.; Ruh, H.; Lee, H. J. *Appl. Phys. Lett.* **2002**, *81*, 3648.
(5) Wang, J. X.; Sun, X. W.; Yang, Y.; Huang, H.; Lee, Y. C.; Tan, O. K.; Vayssieres, L. *Nanotechnology* **2006**, *17*, 4995.
(6) Wei, A.; Sun, X. W.; Wang, J. X.; Lei, Y.; Cai, X. P.; Li, C. M.; Dong, Z. L.; Huang, W. *Appl. Phys. Lett.* **2006**, *89*, 123902.
(7) Zhang, X. M.; Lu, M. Y.; Zhang, Y.; Chen, L. J.; Wang, Z. L. *Adv. Mater.* **2009**, *21*, 2767.
(8) Liu, W. H.; Lee, M.; Ding, L.; Liu, J.; Wang, Z. L. *Nano Lett.* **2010**, *10*, 3084.
(9) Whang, D.; Jin, S.; Wu, Y.; Lieber, C. M. *Nano Lett.* **2003**, *3*, 1255.
(10) Park, J. Y. *Nanotechnology* **2007**, *18*, 095202.
(11) Zhong, Z. H.; Wang, D. L.; Cui, Y.; Bockrath, M. W.; Lieber, C. M. *Science* **2003**, *302*, 1377.
(12) Postma, H. W. C.; Sellmeijer, A.; Dekker, C. *Adv. Mater.* **2000**, *12*, 1299.
(13) Tak, Y.; Yong, K. J. *J. Phys. Chem. B* **2005**, *109*, 19263.
(14) Wei, Y. G.; Wu, W. Z.; Guo, R.; Yuan, D. J.; Das, S. M.; Wang, Z. L. *Nano Lett.* **2010**, *10*, 3414.
(15) Fuhrmann, B.; Leipner, H. S.; Hoche, H. R.; Schubert, L.; Werner, P.; Gosele, U. *Nano Lett.* **2005**, *5*, 2524.
(16) Martensson, T.; Carlberg, P.; Borgstrom, M.; Montelius, L.; Seifert, W.; Samuelson, L. *Nano Lett.* **2004**, *4*, 699.
(17) Zhang, H.; Mirkin, C. A. *Chem. Mater.* **2004**, *16*, 1480.
(18) Wang, W. C. M.; Stoltenberg, R. M.; Liu, S. H.; Bao, Z. N. *ACS Nano* **2008**, *2*, 2135.
(19) Xu, S.; Wei, Y.; Kirkham, M.; Liu, J.; Mai, W.; Davidovic, D.; Snyder, R. L.; Wang, Z. L. *J. Am. Chem. Soc.* **2008**, *130*, 14958.
(20) Zhang, K.; Yang, Y.; Pun, E. Y.; Shen, R. *Nanotechnology* **2010**, *21*, 235602.
(21) Englander, O.; Christensen, D.; Lin, L. *Appl. Phys. Lett.* **2003**, *82*, 4797.
(22) Jungen, A.; Stampfer, C.; Hierold, C. *Appl. Phys. Lett.* **2006**, *88*, 191901.
(23) Zhou, Y.; Johnson, J.; Wu, L.; Maley, S.; Ural, A.; Xie, H. 8th IEEE Conference on Nanotechnology; Arlington, Texas, USA, 18−21 August 2008.
(24) Tong, T.; Li, J. G.; Chen, Q.; Longtin, J. P.; Tankiewicz, S.; Sampath, S. *Sens. Actuators, A* **2004**, *114*, 102.
(25) Takashi, K.; Atsushi, I.; James E., B.; Koichi, H.; Tatsuki, K.; Eiji, M. *Appl. Phys. Lett.* **1986**, *19*, 2160.
(26) Takashi, K.; Atsushi, I.; James E., B.; Koichi, H.; Tatsuki, K.; Eiji, M. *Macromolecules* **1986**, *19*, 2160.
(27) Park, I.; Li, Z. Y.; Pisano, A. P.; Williams, R. S. *Nano Lett.* **2007**, *7*, 3106.
(28) Wolf, S.; Tauber, R. N. *Silicon Processing for the VLSI Era: Process Technology*; 2nd ed.; Lattice Press: Sunset Beach, CA, 1999; Vol. 1.
(29) Campos, L. C.; Dalal, S. H.; Baptista, D. L.; Magalhaes-Paniago, R.; Ferlauto, A. S.; Milne, W. I.; Ladeira, L. O.; Lacerda, R. G. *Appl. Phys. Lett.* **2007**, *90*, 181929.
(30) Luo, L.; Sosnowchik, B. D.; Lin, L. W. *Appl. Phys. Lett.* **2007**, *90*, 093101.
(31) Liu, B.; Zeng, H. C. *J. Am. Chem. Soc.* **2003**, *125*, 4430.
(32) Jiang, X.; Tian, B.; Xiang, J.; Qian, F.; Zheng, G.; Wang, H.; Mai, L.; Lieber, C. M. *Proc. Natl. Acad. Sci. U.S.A.* **2011**, *108*, 12212.
(33) Gao, X. P.; Zheng, G.; Lieber, C. M. *Nano Lett.* **2010**, *10*, 547.